International Journal of Heat and Fluid Flow 50 (2014) 378–385

Contents lists available at ScienceDirect

International Journal of Heat and Fluid Flow

journal homepage: www.elsevier.com/locate/ijhff

Jet impingement in a crossflow configuration: Convective boiling and local heat transfer characteristics

Geehong Choi, Beom Seok Kim, Hwanseong Lee, Sangwoo Shin, Hyung Hee Cho *

Department of Mechanical Engineering, Yonsei University, 50 Yonsei-ro, Seodaemun-gu, Seoul 120-749, Republic of Korea

ARTICLE INFO

Article history:
Received 22 November 2013
Received in revised form 7 August 2014
Accepted 29 September 2014
Available online 18 October 2014

Keywords:
Flow boiling convective heat transfer
Impingement jet
Local temperature measurement
Flow visualization

ABSTRACT

Flow boiling accompanied impingement jet was highly desired to enhance convective heat transfer. The secondary jet impingement system was designed to get enhanced heat transfer performance. The fluidic behavior was analyzed through visualization, and the local heat transfer was evaluated using an array of resistance temperature detector (RTD) sensors. The dielectric fluid FC-72 was used as coolant, and flowed through the rectangular channel with flow rate of Re = 6000 and saturated condition. We confirmed that the jet blowing ratio significantly influenced to the fluidic structure and local heat transfer distributions. Reinforced convective motion by jet flow removed bubbles on the heating surface, and increased local heat transfer coefficient by 59% with decreased wall superheat by 11% at the jet blowing ratio of 1:5. Whereas more intensified convective flow could delay onset of nucleate boiling (ONB) by disturbing thermal boundary layer at the jet blowing ratio of 1:10. Critical heat flux (CHF) increased quasi-linearly by increasing of the jet blowing ratio leading to the reinforcement of total fluidic momentum. Based on the results of the various jet blowing ratios and consequent local/overall heat transfer data, we conclude that the jet blowing ratio of 1:5 is an optimized condition for enhancing heat transfer coefficient at a given exit quality in the tested blowing ratios.

1. Introduction

Boiling heat transfer is an effective cooling technique, as large amounts of heat can be dissipated due to the latent heat of evaporation of the coolant (Chen et al., 2009; Lu et al., 2011). Boiling heat transfer has been used in applications for power plant, refrigeration system, and electronic devices. Boiling can be divided into two categories: pool boiling, which occurs in stationary flow, and flow boiling, which occurs in forced convective flow. In flow boiling, forced convection of the coolant is accompanied by a phase change, which can dissipate large amounts of heat due to the latent heat of evaporation (Hu et al., 2011; Morshed et al., 2012). The convective flow influences the phase change characteristics considerably. The temperature of the working fluid affects the development of the thermal boundary layer (Zou, 2010), and also influences the bubble dynamics near the surface (Jia and Dhir, 2004). Large mass flow rates can remove efficiently bubbles from the heating surface, further increasing the heat flux that can be achieved (Harirchian and Garimella, 2008; Kew and Cornwell, 1997).

Jet impingement is another powerful cooling technique, and has been used to intensify forced convection effects on flow boiling (Cho et al., 2011; Guo et al., 2011). An impinging jet can cool a heating surface using a small amount of coolant; thus, it is an effective technique for cooling local hot spots (Li et al., 2014; Rhee et al., 2003). The heat transfer characteristics of impinging jets have been reported in a number of studies (Cooper et al., 1993; Craft et al., 1993; Hrycak, 1981; Hwang et al., 2001; Li et al., 2013; Livingood and Hrycak, 1973; Shin et al., 2009; Zuckerman and Lior, 2006). Jet impingement can be categorized according to the type of jet; categories include free surface, plunging, submerged, confined, and crossflow jets. However, the flow characteristics are the principal factor affecting flow boiling. The flow characteristics of free surface, submerged, and circular array jets have been investigated by varying the ratio of the jet hole diameter to the distance between the nozzle and surface (Cardenas and Narayanan, 2012; Shin et al., 2008; Wu et al., 2007). The principle feature of jet flow is a concentrated coolant supply at the heating surface. By employing impinging jets in boiling heat transfer, the nucleate boiling region is extended, and the critical heat flux (CHF) can be increased (Li and Liu, 2012). It has been shown that CHF increases with the jet velocity, and the effect of the impinging jet is more significant when the distance between the jet nozzle and the heating surface is small (Katto and Kunihiro, 1973). A semi-empirical

* Corresponding author. Tel.: +82 2 2123 2828; fax: +82 2 312 2159.
E-mail address: hhcho@yonsei.ac.kr (H.H. Cho).

http://dx.doi.org/10.1016/j.ijheatfluidflow.2014.09.010
0142-727X/

Nomenclature

A	area of the heater
a	calibration coefficient
b	calibration coefficient
C	heat capacity
h	heat transfer coefficient
I	current
k	thermal conductivity
L	latent heat
M	jet blowing ratio of secondary jet velocity to main flow velocity
$\dot{m}$	mass flow rate
$\dot{Q}$	heat transfer rate
q''	heat flux
R	resistance
T	temperature
t	thickness of the wafer
V	voltage drop
x	exit quality
δ	boundary layer thickness

Subscripts

e	exit
f	fluid
i	local RTD sensor number
in	inlet
l	liquid
$loss$	loss
net	net
p	constant pressure condition
R	RTD sensor measured
sat	saturated
Si	silicon
s	single phase
t	thermal
w	wall

correlation to predict CHF at various jet impingement conditions was reported by Qiu and Liu (2005).

Despite a number of reports of jet impingement applied to boiling heat transfer, it remains a challenge to achieve a large heat transfer rate. In this study, we applied jet impingement in a cross-flow configuration to flow boiling to investigate the cooling performance. The local heat transfer rates were evaluated using a resistance temperature detector (RTD) array, which was fabricated using micro-electro-mechanical system (MEMS) technology. The dielectric coolant FC-72 was used as the working fluid. The temperature of the fluid was controlled at 56 °C, the saturation temperature of FC-72, to exclude subcooling effects, and the experiments were carried out at atmospheric pressure. In this study, as an experimental variable, the flow conditions were changed by varying the jet blowing ratio, which is the ratio of the secondary jet velocity to the main flow velocity (Amano and Sundén, 2014); the main flow was fixed so that the Reynolds number was 6000 based on main flow velocity. Four different blowing ratios were investigated using the RTD sensor array, and the local heat transfer characteristics were examined.

2. Experimental design

2.1. Experimental system

The experimental system is presented schematically in Fig. 1(a). The main reservoir contained the working fluid. An immersion heater was placed in the working fluid and operated for about 1 h to achieve degassing. The working fluid was maintained at atmospheric pressure. A magnetic pump (TXS5.3, Tuthil Co., CA) and a three-phase motor (LG-OTIS, 0.5 hp, 3500 rpm) were used to pump the working fluid through the closed circulation loop. The motor speed was controlled using an inverter, which was connected to the three-phase motor. The working fluid passed through a flow meter (ULTRA mass MK II, Oval Co.), and the total mass flow rate was monitored using an indicator (FC100P, FLOS Korea Co.). The temperature of the working fluid was controlled using a heat exchanger (Flat-plate, Model 131001694), and maintained closed to 56 °C, which is the saturation temperature of the FC-72 working fluid (3 M). Temperature deviation between the inlet and outlet of channel was less than 0.5 °C, thus the averaged fluid temperature was used as a bulk fluid temperature on the heating surface in the saturated condition. The working fluid was divided into the main flow and the secondary jet flow. The bypass rate was regulated using a flow-control valve, and the mass flow rate of the secondary jet was measured using an additional flow meter (M006-1T1, Autoflow Co.). The electrical signals for measuring the temperature, pressure, and mass flow rates were acquired using a data acquisition system (DAS) composed of an RTD signal module (National Instruments, SCXI-1503) to monitor the temperature distribution and a data logger (Agilent, 3490 A, 20 channels) for the additional parameters. The electric currents were supplied using a power supply (300 V, 10 A, KSC).

The test section was fabricated using acrylic, and assembled into upper and bottom parts to form a fluid-flow channel, as shown in Fig. 1(b). During the experiments, the fluid was contained in the settling chambers installed at the inlet and outlet of the flow channel to stabilize the fluid flow. Temperatures and pressures of the working fluid were measured in those settling chambers using J-type thermocouples (Omega) and pressure gauges (PMP 4070 for absolute pressure, PMP 4170 for differential pressure, GE Druck), respectively. The thermocouples were inserted at mid-height to measure fluid temperature, and covered by hard sheath to prevent bending by fluid flow. The cross-sectional dimensions of the main flow channel were 8 mm × 8 mm in square with hydraulic diameter of 8 mm. The total length of the channel was 375 mm, and the length of the upstream region was 230 mm, which was sufficient for the flow to be fully developed. The jet flowed through a circular aperture with a diameter of 3 mm, located above sensor 1, and passed secondary channel with length of 30 mm, in which the secondary jet flow is sufficient to develop (Cengel et al., 2012). The sides of the test section of the heated region were composed of transparent quartz windows for flow visualization. The test section was covered by a thermally insulating material to reduce heat loss to the environment.

The boiling experiments were conducted by measuring the wall temperatures as functions of the heat flux conditions. The jet blowing ratio was the principal factor characterizing the impinging jet. The main flow was maintained at Re = 6000, and the jet blowing ratio was varied over the range of 0–10.

2.2. RTD sensor fabrication

The RTD array sensor was fabricated on a p-type Si wafer (Boron-doped, (100) orientation, with resistivity in the range of 1–20 Ω cm) using MEMS technology (Kim et al., 2014). Pt was used for the RTD wire patterning because its resistance is proportional

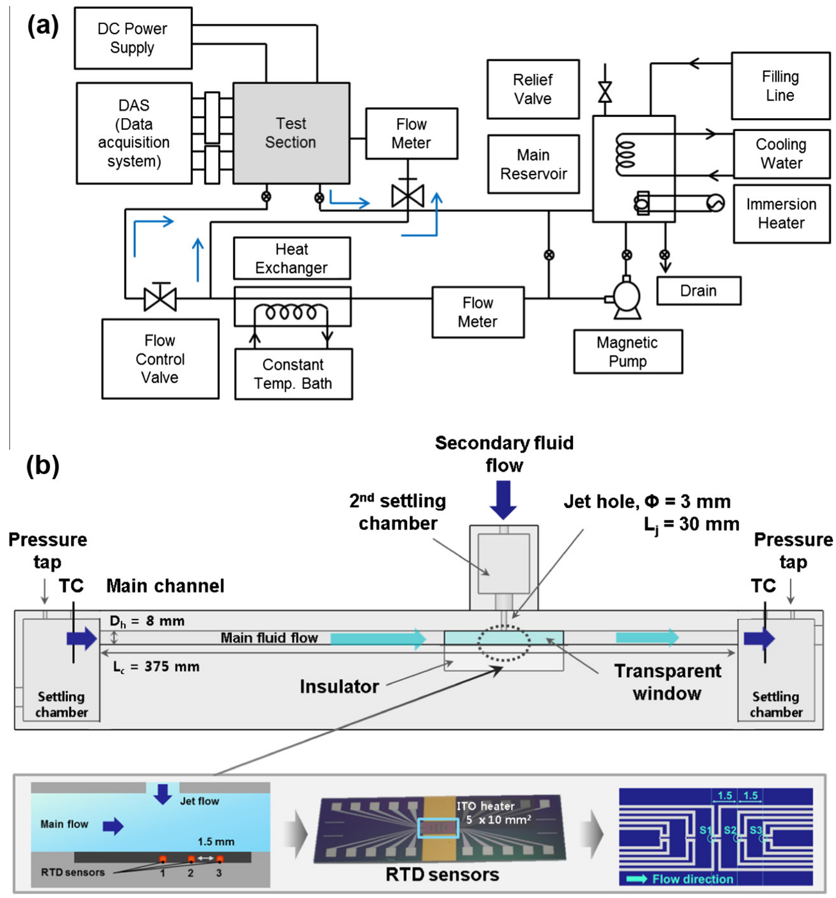

Fig. 1. Schematic diagram of the experimental apparatus: (a) flow boiling experimental system, (b) test section for investigating the flow boiling.

to the temperature. The three points used to measure the resistance were located starting at the center at 1.5 mm intervals in the downstream direction, termed sensors 1, 2, and 3. The resistance of each RTD was over 500 Ω at room temperature to get more sensitive measuring of RTD sensors. An insulation layer was deposited on the Pt sensors, and an indium tin oxide (ITO) heater was defined on top of this insulation layer. Two Au electrodes were patterned on both ends of the ITO heater to supply current, and connected to a copper block on the bottom. Thus, heat was transferred on the opposite side of the wafer to the RTD sensors.

3. Data acquisition

The experimental data were acquired at a sampling rate of 60 Hz using DAS, and then time-averaged at each point. The boiling characteristic curves were evaluated using the data reduction procedures described below.

3.1. Applied heat flux

The applied heat flux from the ITO heater can be calculated from the voltage drop across the heater and the current as follows:

$$q'' = \frac{\dot{Q}}{A} = \frac{V \times I}{A} \quad (1)$$

where $\dot{Q}$ is the heat transfer rate, A is the area of the heater, V is the voltage drop, and I is the current in the heater. When boiling was developed near CHF, local wall temperature was fluctuated unstably more than 20° of centigrade within 1 ms or increased suddenly. The value of CHF was estimated by adding the half of increment between the unstably fluctuated heat flux and the previous heat flux of that (Rainey et al., 2003).

3.2. Wall temperature

The wall temperature distribution was evaluated using the RTD sensor array. The resistance of the RTD sensors was measured at temperatures over the range of 293–329 K, i.e., from room temperature to the boiling point, and calibration relationships for the RTD temperature were obtained at the three resistance detecting points, i.e., $T_{R,i} = a_i \cdot R_i + b_i$, where $T_{R,i}$ is the RTD temperature of sensor i, R_i is the resistance of sensor i, and a_i and b_i are the calibration coefficients. However, the heat transfer surface was on the side of the wafer opposite to the RTD array. The thickness of the silicon substrate was thin of 500 μm compared to the heater size, thus the wall temperature was calculated using Fourier's law for one-dimensional thermal conduction (Chen et al., 2009; Kim et al., 2014; Lu et al., 2011), i.e.,

$$q'' = \frac{k_{Si}}{t}(T_R - T_w) \quad (2)$$

where k_{Si} is the thermal conductivity of the silicon substrate, t is the thickness of the wafer in the direction of the heat flux, T_R is the temperature at the RTDs, and T_w is the wall temperature.

3.3. Heat transfer coefficient

To analyze the spatial dependence of the jet impingement cooling under flow boiling conditions, the local heat transfer coefficients were evaluated based on Newton's law of cooling, which is expressed as follows:

$$q'' = h(T_w - T_f) \quad (3)$$

where T_f is the bulk temperature of the working fluid controlled to the saturated temperature, which was averaged by the inlet and outlet fluid temperatures of the channel. The wall and fluid temperatures were used to determine the local heat transfer coefficient. The fluid temperature was measured at the inlet settling chamber, and was maintained at the saturation temperature of FC-72.

4. Uncertainty analysis

The experimental uncertainties were calculated based on the method proposed by Moffat (1985). Uncertainties in the dimensions and measurements were considered in the evaluation of the main variables. The error in the patterned length of the sensor was ±0.2%, and the error in the temperature measured by the thermocouple was 0.05%. Based on the calibration process of the RTD sensors, an uncertainty of 1.2% was applied to the wall temperature. The calculated Reynolds number had an uncertainty of 0.15%. Conductive heat loss through the silicon substrate was computed using a commercial CFD code, Fluent (ANSYS, version 6.3.26). Effective heating area was evaluated based on the assumption that the area of heat transferred by convection was the same with the area of heat spreading. The heat flux deviation caused by heat spreading was considered as conductive heat loss, the evaluated heat loss was 6.3%. Based on this, the uncertainty of heat flux including CHF was calculated by following equations;

$$\frac{\delta q''}{q''} = \left[\left(\frac{\delta V}{V}\right)^2 + \left(\frac{\delta I}{I}\right)^2 + \left(\frac{\delta A}{A}\right)^2 + \left(\frac{\delta q''_{loss}}{q''}\right)^2\right]^{\frac{1}{2}} \quad (4)$$

voltage drop, current and heating area of the heater were used, and the evaluated uncertainty of the heat flux was 6.4%. The uncertainty of the wall temperature was calculated in the thin silicon substrate, and the investigated wall temperature uncertainty was 6.9%.

$$\frac{\delta h}{h} = \left[\left(\frac{\delta q''}{q''}\right)^2 + \left(\frac{\delta T_w}{T_w}\right)^2 + \left(\frac{\delta T_f}{T_f}\right)^2\right]^{\frac{1}{2}} \quad (5)$$

The uncertainty of the heat transfer coefficient was evaluated considering the deviation of heat flux, wall temperature, and fluid temperature, and the value was 9.4%.

5. Results

The flow boiling curves are plotted in Fig. 2 at the three locations of RTD sensors to analyze the effect of the jet on flow boiling with previous study in convective flow (Yuan et al., 2009) and free surface jet condition (Cardenas and Narayanan, 2012). In the single-phase region, the gradient of the boiling curves increased slightly as the jet blowing ratio increased. The single-phase heat transfer region was extended at higher jet blowing ratios of 1:10, and the onset of nucleate boiling (ONB) was delayed. The intensified forced convection due to the jet flow increased CHF. Wall superheat decreased in a jet blowing ratio of 1:5 at the sensor 3. Low wall superheat at a given heat flux corresponded to high cooling performance. The wall superheating was related to the heat transfer coefficient using Eq. (3).

The heat transfer coefficient is an important indicator of the heat transfer characteristics. The local heat transfer coefficient can be evaluated based on the boiling curves. Fig. 3(a) shows the distribution of local two-phase heat transfer coefficients from the sensors 1 and 3 as functions of the heat flux, and Fig. 3(b) shows

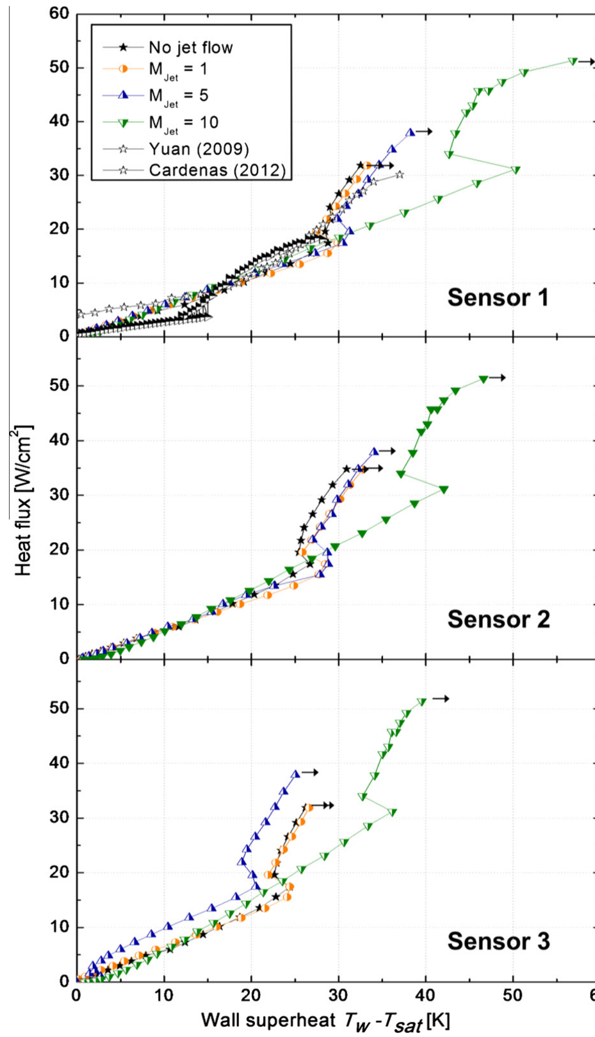

Fig. 2. Local flow boiling curves at the three sensors according to the jet blowing ratio (M_{Jet} means the jet blowing ratio of secondary jet velocity to main flow velocity). The sensor 1 is positioned under the jet hole, and other sensors are arrayed with the interval of 1.5 mm. "No jet flow" means that only the main flow was used.

these as functions of the exit quality, x_e. As the main flow passed the heating surface, the boiling development was suppressed at the upstream compared to the downstream from the heater. Thus, phase change occurred actively by fully developed thermal boundary layer in the downstream region, and the local heat transfer coefficient increased along the flow direction. As shown in Fig. 3(a), a greater heat flux is required to achieve boiling at higher jet blowing ratios; thus, the curves are shifted to the right at high jet blowing ratios. The exit quality represents the amount of boiling (Megahed, 2012), and can be used to compare the heat transfer performance at the same boiling condition but different mass flow rates. It is defined as follows:

$$x_e = \frac{1}{L}\left[\frac{Q_{net}}{\dot{m}} - C_p(T_{sat} - T_{in})\right] \quad (6)$$

where L is the latent heat, Q_{net} is total supplied heat, $\dot{m}$ is the mass flow rate, and C_p is the heat capacity. Therefore, the effect of the impinging jet can be compared at a given exit quality, which improves the heat transfer coefficient as the jet blowing ratio is increased. However, the measured heat transfer coefficient at the sensor 3 for a jet blowing ratio of 1:5 was significantly higher than that for a jet blowing ratio of 1:10 even though the injected mass

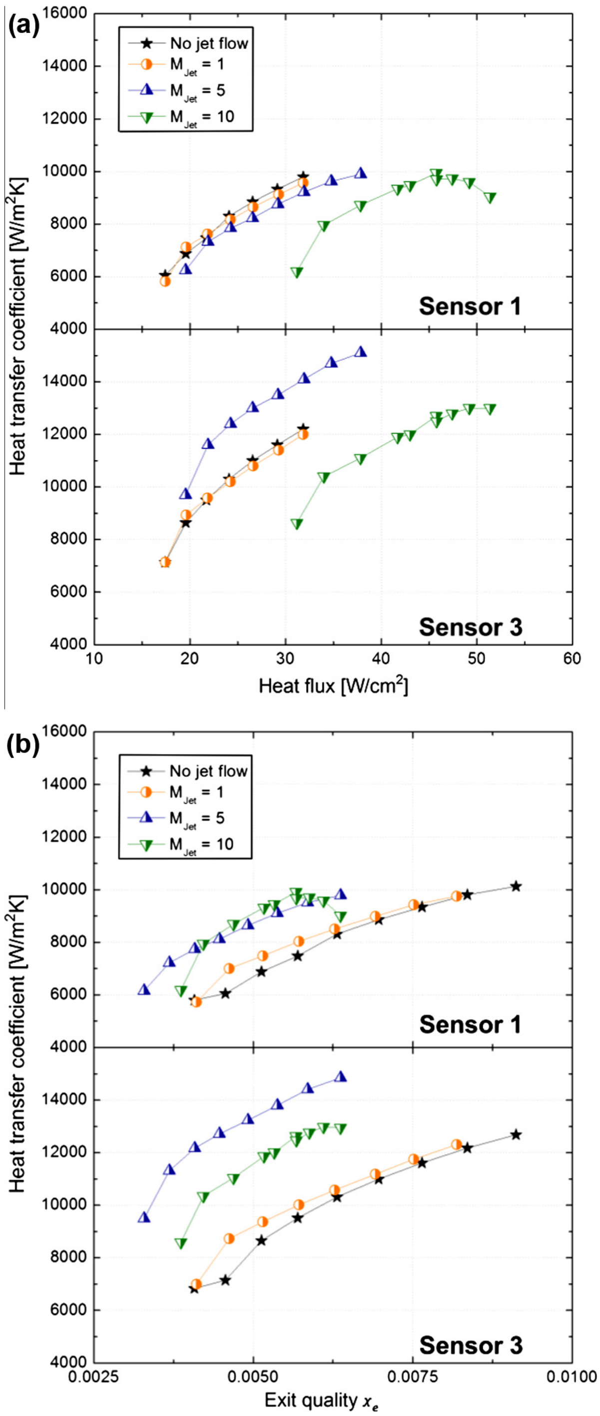

Fig. 3. Distribution of heat transfer coefficients at two sensors: (a) as a function of the heat flux, (b) as a function of the exit quality.

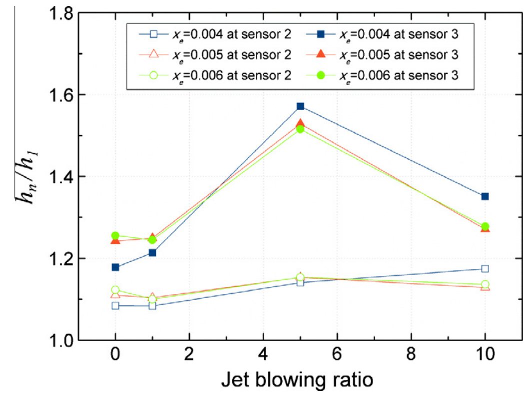

Fig. 4. Ratio between the heat transfer coefficient at sensors 2 and 3 compared with that at sensor 1 as functions of the jet blowing ratio as boiling developed.

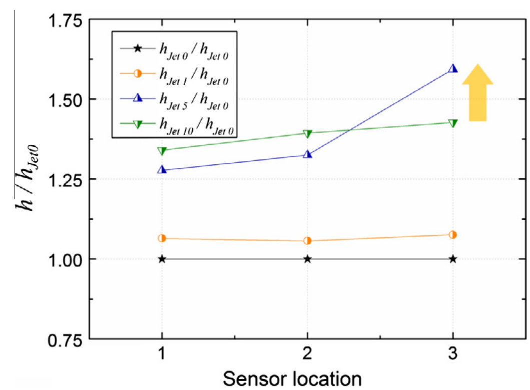

Fig. 5. Variation of the heat transfer coefficients compared to the case with no jet flow for the three different jet blowing ratios and at three sensors. h_{jet0} is the heat transfer coefficient with no jet flow and sensors 1, 2, and 3 are arrayed from the center in the downstream direction.

flow rate less. Fig. 4 represents the ratio of the local heat transfer coefficients at the sensors 2 and 3 to that at the sensor 1. The heat transfer coefficient at the sensor 2 did not change significantly with the jet blowing ratio or exit quality. On the other hand, the heat transfer coefficient at the sensor 3 changed obviously, and was the largest at a jet blowing ratio of 1:5.

To evaluate the enhanced heat transfer by jet, the change in the heat transfer coefficient compared to the case with no jet flow is shown in Fig. 5. The presented two-phase heat transfer coefficient was averaged over the exit quality range of $0.004 < x_e < 0.006$. The local heat transfer coefficient was increased by the jet due to the intensified forced convection. As the jet blowing ratio increased, the mass flow rate of the working fluid at the heated surface also increased. At the sensor 3, the average two-phase heat transfer coefficient was increased by 59% and wall superheat was maintained relatively lower by 11% in a jet blowing ratio of 1:5 compared to the case with no jet. The jet blowing ratio of 1:5 provided the greatest improvement in the cooling performance at the sensor 3, better than the case with a jet blowing ratio of 1:10, and consistent with the $x_e{-}h$ distribution as shown in Fig. 3(b). The maximum heat transfer coefficient at the sensor 3 at a jet blowing ratio of 1:5 was 16% greater than that in a jet blowing ratio of 1:10. Based on the heat transfer coefficient distribution, the cooling performance was not proportional to the jet blowing ratio, and a jet blowing ratio 1:5 had the highest local heat transfer coefficient at the sensor 3 for the tested conditions.

To gain further insight into the heat transfer phenomena, we carried out visualizations of fully developed boiling at a heat flux of 20 W/cm^2 with a high speed camera of 4000 fps. The gray box with arrow described in Fig. 6 is the location of jet hole, and the small white squares indicate the location of sensors. The dot line indicates interfacial boundary forced by the mainstream and the jet flow. As shown in the visualization results, the impingement point of the jet at a jet blowing ratio of 1:5 occurred at the sensor 3; therefore, this point was cooled effectively by impingement jet flow. The large coolant momentum due to the high mass flow rate intensified the forced convection, and the jet flow catalyzes bubble detachment. When the jet blowing ratio was 1:10, the jet flow was dominant and the main flow was not sufficient to control the flow

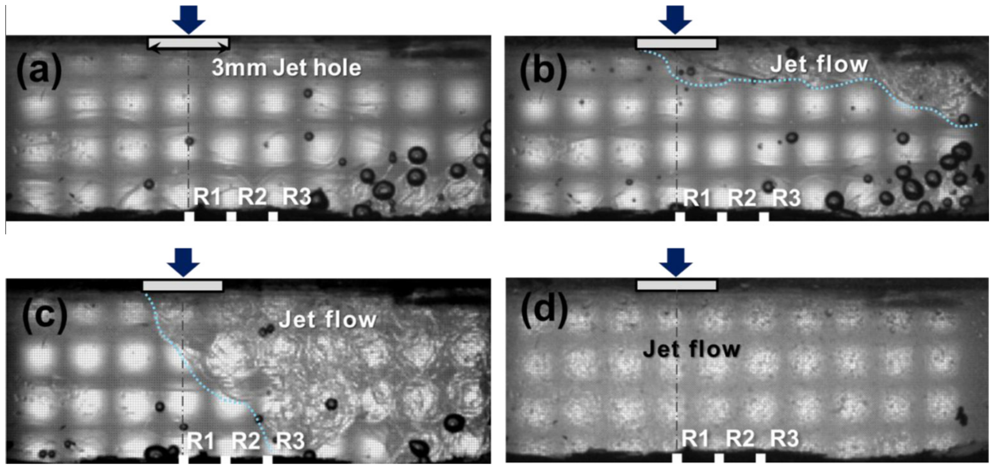

Fig. 6. Visualizations of the flow at a heat flux of 20 W/cm^2. The gray box with arrow indicates the location of the jet nozzle, and the small white squares indicate the locations of sensors. The dotted line indicates the interface between the main flow and the jet flow. (a) No jet flow, (b) jet blowing ratio of 1:1, (c) jet blowing ratio of 1:5, (d) jet blowing ratio of 1:10.

momentum near the heating surface. For this reason, bubble detachment in the downstream direction was minimal. The ratio of the heat transfer coefficient increased with the jet blowing ratio. The jet flowed in the crossflow direction and merged with the main flow, which led to increase thermal transport at the sensor 3 compared with that at the sensors 1 and 2. Therefore, the change in the heat transfer rate was the largest at a jet blowing ratio of 1:5. At this jet flow condition, the jet momentum was the greatest at the sensor 3, and the jet promoted bubble detachment. Forced convection improved bubble nucleation, and cooling performance was maximized.

These flow characteristics influenced the overall boiling heat transfer. Fig. 7 shows ONB and CHF evaluated from the averaged data from the three sensors as functions of the total mass flow rate. The total mass flow rate is the summation of the main flow rate and the impinging jet flow rate. The CHF was enhanced quasi-linearly by increasing the total mass flow rate, and increased by 61% at a jet blowing ratio of 1:10 compared to the case with no jet flow. This was because a greater heat flux could be transferred by the larger amount of coolant. However, ONB did not change until the total flow rate reached of 2.0 kg/min, which corresponds to a jet blowing ratio of 1:5, at which point it increased rapidly by 61% at a total mass flow rate 2.8 kg/min, which corresponds to a jet blowing ratio of 1:10. The reason that ONB increased so sharply can be explained by considering the fluid flow behavior using the visualization data. A phase change was not initiated at the heat flux of 20 W/cm^2 in a jet blowing ratio of 1:10, and bubbles were not observed in Fig. 6(d). When the jet velocity was zero, only the main flow existed in the channel, as shown in Fig. 6(a). Fig. 6(b) shows the flow when the jet velocity was equal to the main flow and the jet flow was injected from the ceiling of the channel. The jet flow at a blowing ratio of 1:1 did not significantly affect the heat transfer at the heating surface as the amount of jet flow was small

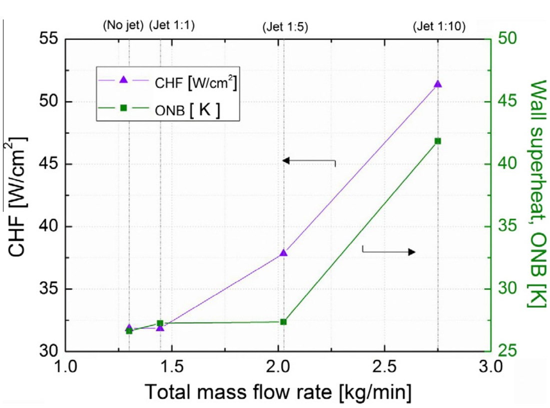

Fig. 7. Boiling heat transfer characteristics for the average data of three sensors as functions of the total mass flow rate.

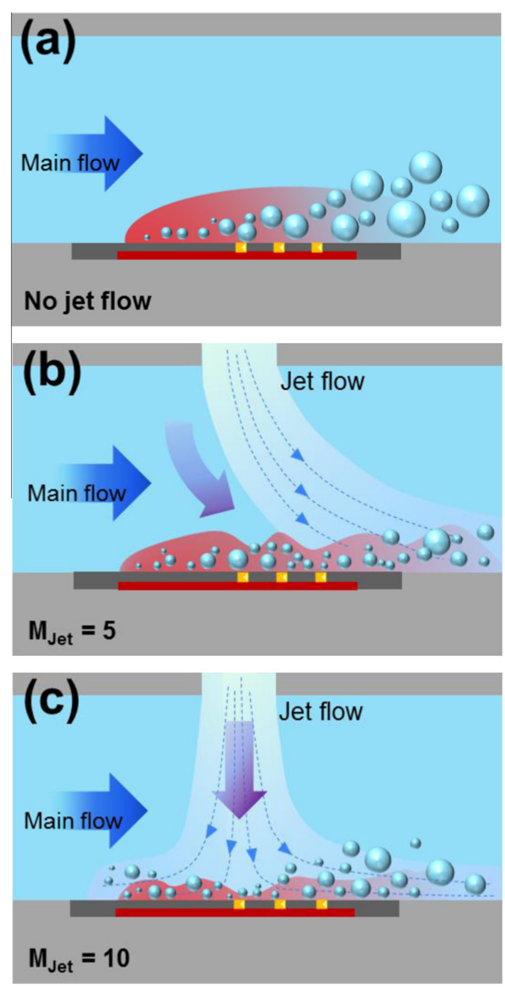

Fig. 8. Schematic diagram illustrating the effect of the impinging jet on flow boiling. (a) No jet flow, (b) jet blowing ratio of 1:5, (c) jet blowing ratio of 1:10.

compared to the amount of main flow. However, at a jet blowing ratio of 1:5, the jet impinged on the heating surface close to the sensor 3. When the total mass flow rate was less than 2.0 kg/min, the jet did not impinge on the heating surface, and the nucleate convection was affected by the main flow only. At a jet blowing ratio of 1:10, the jet flow was dominant and impinged on the whole heating surface. The temperature profile in thermal boundary layer of boiling has been assumed that it is distributed linearly as Zuber (Zuber, 1959) suggested. Based on the assumption, the thickness of thermal boundary layer can be estimated through Eq. (7) (Basu et al., 2002; Chang et al., 2010; Kandlikar, 2006; Li et al., 2008). Thus the intensified jet flow increased the single-phase heat transfer coefficient, and resulted in a thin thermal boundary layer.

$$\delta_t = \frac{k_l}{h_S} \tag{7}$$

where k_l is the thermal conductivity of the liquid and h_S is the single-phase heat transfer coefficient. A thin thermal boundary layer requires a larger wall superheat to cause a phase change of the working fluid (Hsu, 1962). Therefore, the disturbed flow caused by the large jet flow ratio of 1:10 delayed ONB, and CHF was enhanced due to the increased total mass flow rate.

A thermal boundary layer developed in the direction of the main flow, and boiling occurred as described by the schematic diagrams shown in Fig. 8. As discussed before, the properly combined impingement jet and duct flow removes bubble effectively on the local heating surface, thus heat transfer coefficient become the highest at the jet blowing ratio of 1:5. Therefore, the combined heat transfer by impingement jet and duct flow occurred most remarkably with the jet blowing ratio of 1:5 compared to the other jet blowing ratios.

6. Conclusion

For the application of jet impingement to forced convective boiling, we tried to design a secondary jet impingement system which is favorable to enhance overall and local heat transfer performances. Local heat transfer and bubble flow characteristics were experimentally evaluated using local temperature-measuring RTD array sensors and high speed camera, respectively. Based on these experimental results, we analyzed jet induced fluidic behaviors over a heat transfer surface. Jet blowing ratio, which is the velocity ratio of secondary jet to mainstream, was a principal factor on local heat transfer characteristics as well as overall boiling performances. The jet blowing ratio was critical to determine the fluidic structure with regard to stagnant behavior of impingement jet, and it consequently dominated the local heat transfer distributions. As the jet blowing ratio increased, the single-phase region was significantly extended to the local upstream region of heater due to reinforced convective motion by jet flow. Concentrated jet momentum in the jet blowing ratio of 1:5 could catalyze bubble detachment more effectively, and lead to low wall superheat by 11% with increased local heat transfer coefficient by 59% compared to no jet condition. However, when the jet disturbed the development of thermal boundary layer over the heating surface, ONB was retarded. Especially under the excessive jet blowing ratio of 1:10, heating region was totally disturbed by strong stagnant fluidic behavior, therefore ONB was remarkably delayed. On the other hand, CHF quasi-linearly increased according to the increase of jet blowing ratio leading to the reinforcement of total fluidic momentum. Based on the demonstrated results about the jet blowing ratio and consequent local/overall heat transfer, we suggest that the jet blowing ratio of 1:5 is an optimal condition for enhancing heat transfer coefficient at a given exit quality. Moreover, this improved convective heat transfer technique can be potentially used to enhance cooling capacity at large heat generated system such as power plant, refrigeration system, and electric devices.

Acknowledgements

This work was supported by a National Research Foundation of Korea (NRF) grant funded by the South Korea government (MEST) (No. 2011-0017673) and the Human Resources Development program (No. 2014030200560) of the Korea Institute of Energy Technology Evaluation and Planning (KETEP) grant funded by the South Korea government Ministry of Trade, Industry and Energy.

References

Amano, R.S., Sundén, B., 2014. Impingement Jet Cooling in Gas Turbines. WIT Press p.

Basu, N., Warrier, G.R., Dhir, V.K., 2002. Onset of nucleate boiling and active nucleation site density during subcooled flow boiling. J. Heat Transfer 124, 717.

Cardenas, R., Narayanan, V., 2012. Heat transfer characteristics of submerged jet impingement boiling of saturated FC-72. Int. J. Heat Mass Transfer 55, 4217–4231.

Cengel, Y.A., Cimbala, J.M., Turner, R.H., 2012. Fundamentals of Thermal-Fluid Sciences, fourth ed. Mc Graw Hill.

Chang, W.R., Chen, C.A., Ke, J.H., Lin, T.F., 2010. Subcooled flow boiling heat transfer and associated bubble characteristics of FC-72 on a heated micro-pin-finned silicon chip. Int. J. Heat Mass Transfer 53, 5605–5621.

Chen, R., Lu, M.-C., Srinivasan, V., Wang, Z., Cho, H.H., Majumdar, A., 2009. Nanowires for enhanced boiling heat transfer. Nano Lett. 9, 548–553.

Cho, H.H., Kim, K.M., Song, J., 2011. Applications of Impingement Jet Cooling Systems. Nova Science Publishers, Inc.

Cooper, D., Jackson, D.C., Launder, B.E., Liao, G.X., 1993. Impinging jet studies for turbulence model assessment—I. Flow-field experiments. Int. J Heat Mass Transfer 36, 2675–2684.

Craft, T.J., Graham, L.J.W., Launder, B.E., 1993. Impinging jet studies for turbulence model assessment—II. An examination of the performance of four turbulence models. Int. J. Heat Mass Transfer 36, 2685–2697.

Guo, D., Wei, J.J., Zhang, Y.H., 2011. Enhanced flow boiling heat transfer with jet impingement on micro-pin-finned surfaces. Appl. Therm. Eng. 31, 2042–2051.

Harirchian, T., Garimella, S.V., 2008. Microchannel size effects on local flow boiling heat transfer to a dielectric fluid. Int. J. Heat Mass Transfer 51, 3724–3735.

Hrycak, P., 1981. Heat transfer from impinging jets – A literature review. NASA report AFWAL-TR-81-3054.

Hsu, Y.Y., 1962. On the size range of active nucleation cavities on a heating surface. J. Heat Transfer 84, 207–213.

Hu, X., Lin, G., Cai, Y., Wen, D., 2011. Experimental study of flow boiling of FC-72 in parallel minichannels under sub-atmospheric pressure. Appl. Therm. Eng. 31, 3839–3853.

Hwang, S.D., Lee, C.H., Cho, H.H., 2001. Heat transfer and flow structures in axisymmetric impinging jet controlled by vortex pairing. In. J. Heat Fluid Flow 22, 293–300.

Jia, W., Dhir, V.K., 2004. Dynamics of contact angle during growth and liftoff of bubbles at a single nucleation site in flow boiling. International Mechanical Engineering Congress and Exposition, IMECE2004-60374.

Kandlikar, S.G., 2006. Nucleation characteristics and stability considerations during flow boiling in microchannels. Exp. Therm. Fluid Sci. 30, 441–447.

Katto, Y., Kunihiro, M., 1973. Study of the mechanism of burn-out in boiling system of high burn-out heat flux. Japan Soc. Mech. Eng. 16, 1357–1366.

Kew, P.A., Cornwell, K., 1997. Correlations for the prediction of boiling heat transfer in small-diameter channels. Appl. Therm. Eng. 17, 705–715.

Kim, B.S., Shin, S., Lee, D., Choi, G., Lee, H., Kim, K.M., Cho, H.H., 2014. Stable and uniform heat dissipation by nucleate-catalytic nanowires for boiling heat transfer. Int. J. Heat Mass Transfer 70, 23–32.

Li, C., Wang, Z., Wang, P.-I., Peles, Y., Koratkar, N., Peterson, G.P., 2008. Nanostructured copper interfaces for enhanced boiling. Small 4, 1084–1088.

Li, Y.-Y., Liu, Z.-H., 2012. Theoretical research of critical heat flux in subcooled impingement boiling on the stagnation zone. Int. J. Heat Mass Transfer 55, 7544–7551.

Li, Y.-Y., Liu, Z.-H., Wang, G.-S., Pang, L., 2013. Experimental study on critical heat flux of high-velocity circular jet impingement boiling on the nano-characteristic stagnation zone. Int. J. Heat Mass Transfer 67, 560–568.

Li, Y.-Y., Liu, Z.-H., Wang, Q., 2014. Experimental study on critical heat flux of steady boiling for high-velocity slot jet impinging on the stagnation zone. Int. J. Heat Mass Transfer 70, 1–9.

Livingood, J.N.B., Hrycak, P., 1973. Impingement heat transfer from turbulent air jets to flat plates – a literature survey. NASA technical memorandum NASA TM X-2778.

Lu, M.-C., Chen, R., Srinivasan, V., Carey, V.P., Majumdar, A., 2011. Critical heat flux of pool boiling on Si nanowire array-coated surfaces. Int. J. Heat Mass Transfer 54, 5359–5367.

Megahed, A., 2012. Local flow boiling heat transfer characteristics in silicon microchannel heat sinks using liquid crystal thermography. Int. J. Multiphase Flow 39, 55–65.
Moffat, R.J., 1985. Using uncertainty analysis in the planning of an experiment. J. Fluids Eng. 107, 173–178.
Morshed, A.K.M.M., Yang, F., Ali, M.Y., Khan, J.A., Li, C., 2012. Enhanced flow boiling in a microchannel with integration of nanowires. Appl. Therm. Eng. 32, 68–75.
Qiu, Y., Liu, Z., 2005. Critical heat flux of steady boiling for saturated liquids jet impinging on the stagnation zone. Int. J. Heat Mass Transfer 48, 4590–4597.
Rainey, K.N., You, S.M., Lee, S., 2003. Effect of pressure, subcooling, and dissolved gas on pool boiling heat transfer from microporous surfaces in FC-72. J. Heat Transfer 125, 75.
Rhee, D.-H., Yoon, P.-H., Cho, H.H., 2003. Local heat/mass transfer and flow characteristics of array impinging jets with effusion holes ejecting spent air. Int. J. Heat Mass Transfer 46, 1049–1061.
Shin, C.H., Kim, K.M., Lim, S.H., Cho, H.H., 2009. Influences of nozzle-plate spacing on boiling heat transfer of confined planar dielectric liquid impinging jet. Int. J. Heat Mass Transf. 52, 5293–5301.
Shin, C.H., Wu, S.J., Kim, K.M., Cho, H.H., 2008. Effects of planar jet impingement on sigle-phase convection and boiling heat transfer characteristics. JP J. Heat Mass Transfer 2, 55–71.
Wu, S.-J., Shin, C.H., Kim, K.M., Cho, H.H., 2007. Single-phase convection and boiling heat transfer: confined single and array-circular impinging jets. Int. J. Multiph. Flow 33, 1271–1283.
Yuan, M., Wei, J., Xue, Y., Fang, J., 2009. Subcooled flow boiling heat transfer of FC-72 from silicon chips fabricated with micro-pin-fins. Int. J. Therm. Sci. 48, 1416–1422.
Zou, L., 2010. Experimental study of subcooled flow boiling on heating surfaces with different thermal conductivities, Collage of Nulcear Engineering. University of Illinois at Urbana-Champaign, Urbana, Illinois.
Zuber, N., 1959. Hydrodynamic Aspects of Boiling Heat Transfer (thesis). Other Information: Orig. Receipt Date: 31-DEC-60, p. Medium: ED; Size: Pages: 210.
Zuckerman, N., Lior, N., 2006. Jet impingement heat transfer: physics, correlations, and numerical modeling. Adv. Heat Transfer 39, 565–631.